

Sequential Latin Hypercube Design for Two-layer Computer Simulators

Yan Wang^{*}, Dianpeng Wang[†], Xiaowei Yue[‡]

Abstract

The two-layer computer simulators are commonly used to mimic multi-physics phenomena or systems. Usually, the outputs of the first-layer simulator (also called the inner simulator) are partial inputs of the second-layer simulator (also called the outer simulator). How to design experiments by considering the space-filling properties of inner and outer simulators simultaneously is a significant challenge that has received scant attention in the literature. To address this problem, we propose a new sequential optimal Latin hypercube design (LHD) by using the maximin integrating mixed distance criterion. A corresponding sequential algorithm for efficiently generating such designs is also developed. Numerical simulation results show that the new method can effectively improve the space-filling property of the outer computer inputs. The case study about composite structures assembly simulation demonstrates that the proposed method can outperform the benchmark methods.

Keywords: Maximin criterion; Optimal LHD; Gaussian process; Principal component scores; Composites structures assembly processes

^{*}Y. Wang is with the School of Statistics and Data Science, Faculty of Science, Beijing University of Technology, Beijing, China (e-mail: yanwang@bjut.edu.cn)

[†](*Corresponding author: Dianpeng Wang*). D. Wang is with School of Mathematics and Statistics, Beijing Institute of Technology, Beijing, China (e-mail: wdp@bit.edu.cn)

[‡]X. Yue is with the Grado Department of Industrial and Systems Engineering, Virginia Tech, Blacksburg, VA, 24061 USA (e-mail: xwy@vt.edu)

1 Introduction

Computer experiments are widely used to emulate physical systems. In practice, one engineering system often contains multi-layer subsystems because of its multi-physics mechanisms or phenomena; the output of one subsystem could be the input for its sequential subsystem. For example, in the earthquake–tsunami model, outputs from the earthquake model are part of the inputs of the tsunami model (Ulrich et al., 2019); the ocean–atmosphere dynamics couples the atmospheric model with the ocean model (Nicholls and Decker, 2015); in the multistage manufacturing processes (MMP), the product quality variations can propagate from one station to its downstream stations (Shi, 2006). Computer experiments for multi-layer physical systems are challenging due to their high complexity. Two-layer systems exist in large numbers in practice and are also fundamental modules for multi-layer ones. Therefore, this work focuses on two-layer computer experiments.

Composite structure assembly is ubiquitous in many industries, such as aerospace, automotive, energy, construction, etc. To mimic the composite structures assembly process, a computer simulation platform was built based on ANSYS PrepPost Composites workbench (Wen et al., 2018, 2019), and it has been calibrated via physical experiments (Wang et al., 2020). This computer simulation can conduct virtual assembly to illustrate detailed composite structure joins, and lay a solid foundation for digital twin simulation of composites assembly. As shown in Figure 1, the virtual assembly simulation includes two computer models. Specifically, the first layer computer model, named the Automatic Optimal Shape Control (AOSC) system, simulates the shape control of a single composite structure (Yue et al., 2018). The AOSC can adjust the dimensional deviations of one composite fuselage and make it align well with the other fuselage to be assembled. The second layer computer model simulates the process of composite structures assembly, where the inputs are critical dimensions from two parts, and the outputs are internal stress after assembly (Wen et al.,

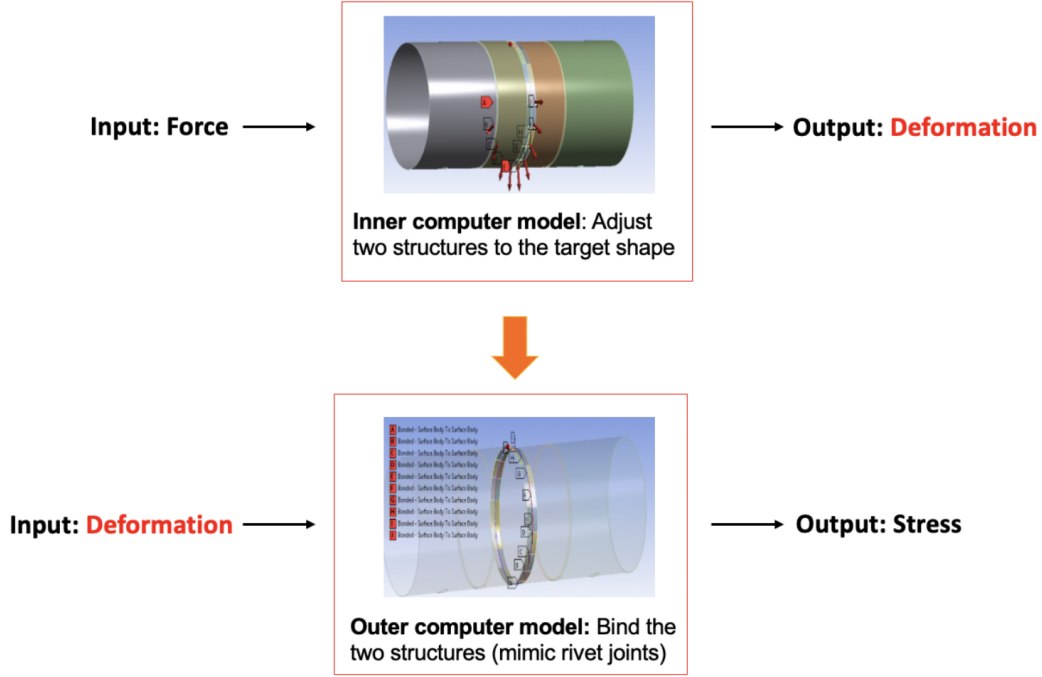


Figure 1: The computer experiment mimics the composite structures assembly process.

2019). Obviously, the inputs of the second layer simulator contain the outputs of the first layer simulator. In practices, the first layer simulator is called the inner computer model, and the second layer one the outer computer model.

In practice, it is commonly believed that design points should be evenly spread in the experimental space to achieve comprehensive exploration. Thus, in the literature, the most commonly used experimental design currently for computer experiments is the space-filling design, such as the Latin hypercube design (LHD) (Santner et al., 2018), the maximin Latin hypercube design (MmLHD) (Joseph and Hung, 2008), and the rotated sphere packing design (He, 2019) etc. However, for the two-layer computer experiments, the one-shot space-filling design is not appropriate. Since a one-shot space-filling design means that the space-filling design is applied only to the inputs of the inner computer model. Inputs to the outer computer model are partly determined by the outputs from the inner computer model. The complexity and non-linearity of the inner computer model may

yield uneven inner computer outputs, thus producing a poor design for the outer computer model. As shown in Figure 2 (details about the inner and the outer computer models can be found in Example 1, Section 4), some of the inner computer outputs are extremely close. This poor design for the outer computer experiments will result in imprecise uncertainty

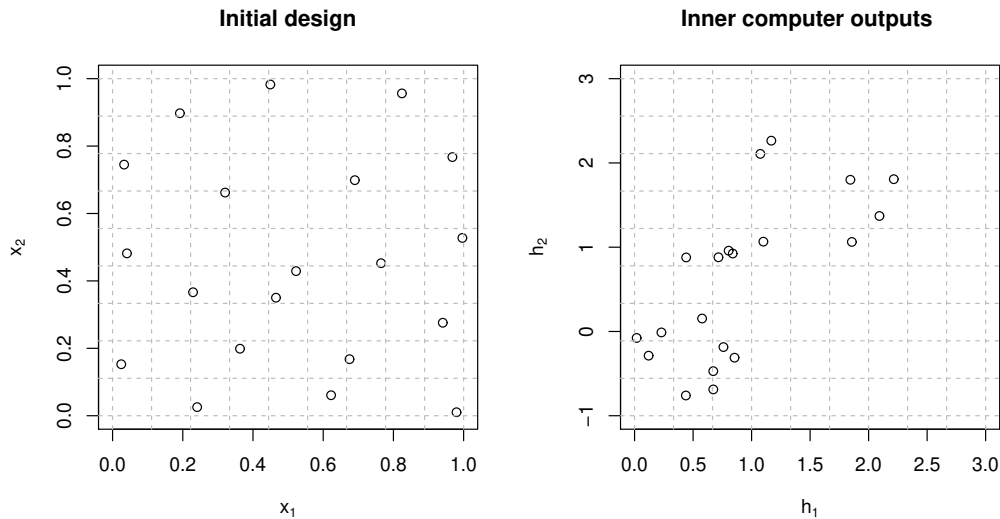


Figure 2: Left: Inputs to the inner computer model (MmLHD); Right: Inner computer outputs.

quantification for the outer computer model. Therefore, it is important to develop new designs for two-layer computer experiments.

Kyzyurova et al. (2018) adopted the space-filling designs for the inner and outer computer experiments separately. This method treats the outputs of the inner computer trial as control variables for the outer trial design, which has three problems: (1) the design region for these control variables is difficult to determine; (2) the outer computer trial ignores the information provided by the inner computer trial; and (3) the method is only applicable to the case where the inner and outer computer trials can be performed independently. For the two-layer computer trials that cannot be performed independently, the scheme cannot be implemented. Marque-Pucheu et al. (2019) and Ming and Guillas (2021) adaptively

generated a sequential optimal design for a two-layer computer model based on a nested Gaussian process model, which assumes that both the inner and outer computer experiments are implementations of the Gaussian process. This kind of approaches are highly dependent on the Gaussian assumptions made about the inner and the outer computer model.

In this work, in order to deal with the challenge of experiments for the two-layer computer experiments, we derive a new distance metric for the inputs of the outer simulator and propose an efficient sequential design scheme by maximizing the minimum new distance between the inputs of the outer simulator. The proposed design can consider the space-filling property of both the inputs and the outputs for the inner computer experiments. Our contributions can be summarized as follows:

- A new distance named the *Mixed-distance* is introduced to measure the inter-site distance between the inputs of the outer computer simulator. This distance is a weighted average of the inter-site distance between the inner computer inputs and the inter-site distance between the inner computer outputs.
- For the multi-response inner computer model, principal component analysis is adopted to reduce the dimensionality of the inner computer outputs. Independent Gaussian Process models (Santner et al., 2018) are built to mimic the principal component scores. The distance between the principal component scores is used to measure the distance between the inner computer outputs. The closed form for this distance can be derived.
- Conventional space-filling design algorithms with deterministic distances are not sufficient when the inputs of the outer model are unknown. To overcome this challenge, the proposed distance between the inner computer outputs considers the uncertainty of the surrogate models. The proposed design can dive into the internal nested struc-

ture and achieve the optimal space-filling properties for both the inner computer model and the outer computer model.

- The Maximin design criterion and a fast algorithm are proposed to generate sequential designs for the two-layer computer experiments. The performance of the proposed method is shown in numerical studies. The proposed method is applied to generate designs for the composite structures assembly experiments.

The outline of this paper is as follows. Section 2 introduces two-layer computer experiments. Section 3 presents the proposed sequential design and gives the detailed algorithm. Section 4 examines the performance of the proposed method through two numerical studies. In Section 5, the proposed method is applied to generate the design for the composite structures assembly simulation. Concluding remarks and the discussions are given in Section 6.

2 Two-layer Computer Experiments

Denote $f : [0, 1]^K \rightarrow \mathbb{R}^M$ to be a deterministic two-layer computer model, which is defined as

$$f(\mathbf{x}) = \mathbf{g} \left(\begin{bmatrix} \mathbf{x} \\ \mathbf{h}(\mathbf{x}) \end{bmatrix} \right), \mathbf{x} \in [0, 1]^K, \quad (1)$$

where $\mathbf{h}(\mathbf{x}) = [h_1(\mathbf{x}), \dots, h_L(\mathbf{x})]^T$ is the $L \times 1$ vector of the inner computer outputs, and $\mathbf{g}(\mathbf{x}^{outer}) = [g_1(\mathbf{x}^{outer}), \dots, g_M(\mathbf{x}^{outer})]^T$ is the $M \times 1$ vector of the outer computer outputs, with $\mathbf{x}^{outer} = [\mathbf{x}^T, \mathbf{h}^T(\mathbf{x})]^T \in [0, 1]^K \times \mathbb{R}^L$ an input of the outer computer model. Here, we assume the outputs for both the inner and outer computer models are scalar. In fact, in many cases, the functional outputs can be discretized to scalar outputs (Chen et al., 2021). It is worth noticing that the design variables in the model (1) are the combinations of all control variables. The two-layer computer model (1) contains the following cases: (1)

$f(\mathbf{x}) = \mathbf{g}(\mathbf{h}(\mathbf{x}))$, in which \mathbf{g} depends on \mathbf{x} only through \mathbf{h} ; (2) \mathbf{x} can be divided into two parts, i.e., $\mathbf{x} = (\mathbf{x}_1, \mathbf{x}_2)$ and $f(\mathbf{x}) = \mathbf{g}([\mathbf{x}_2^T, \mathbf{h}^T(\mathbf{x}_1)]^T)$ (or $f(\mathbf{x}) = \mathbf{g}([\mathbf{x}^T, \mathbf{h}^T(\mathbf{x}_1)]^T)$) as shown in Marque-Pucheu et al. (2019) and Wang et al. (2022). In these cases, the inner computer model $\mathbf{h}(\cdot)$ is insensitive to part of the input variables.

Suppose $\mathbf{X}_n = \{\mathbf{x}_1, \dots, \mathbf{x}_n\}$ is a n -point experiment design, with $\mathbf{x}_i \in [0, 1]^K$. Let $\mathbf{H}_l = [h_l(\mathbf{x}_1), \dots, h_l(\mathbf{x}_n)]^T$, $l = 1, \dots, L$ denote the $n \times 1$ vector of the corresponding responses of $h_l(\cdot)$, and $\mathbf{Y}_I = [\mathbf{H}_1, \dots, \mathbf{H}_L]$ denote the $n \times L$ matrix of the inner computer outputs. Let $\mathbf{X}_n^{outer} = \{\mathbf{x}_i^{outer}\}_{i=1}^n$ denote the set of inputs of the outer computer model and $\mathbf{G}_m = [g_m(\mathbf{x}_1^{outer}), \dots, g_m(\mathbf{x}_n^{outer})]^T$, $m = 1, \dots, M$ the $n \times 1$ vector of the corresponding m -th outer computer outputs and $\mathbf{Y}_O = [\mathbf{G}_1, \dots, \mathbf{G}_M]$ denote the $n \times M$ matrix of the outer computer outputs. Figure 3 shows the framework of two-layer computer experiments.

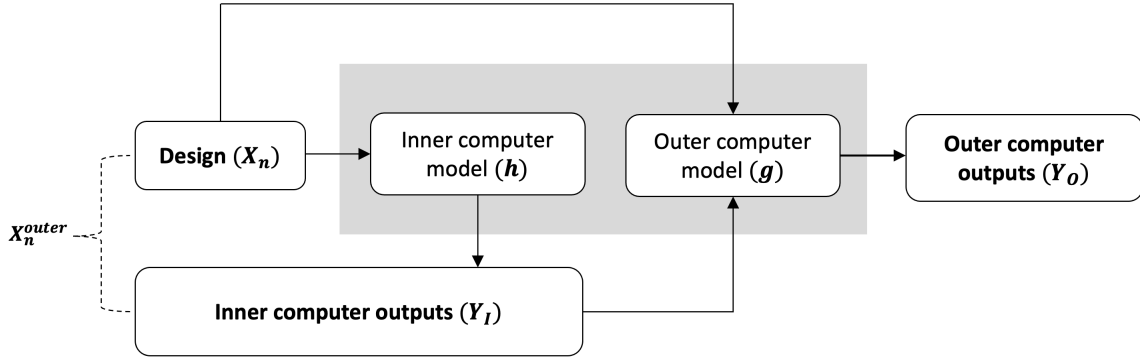


Figure 3: Two-layer computer experiments.

Assume that both the inner and the outer computer models are deterministic but expensive to evaluate. The ‘deterministic’ here refers to that the same input will deduce the same computer output. As discussed above, a one-shot space-filling design \mathbf{X}_n may yield uneven inputs to the outer computer model. To fully explore, optimize or gain insight into the system, the space-filling properties of both the inner computer experimental design and the outer computer inputs need to be considered. That is, an essential consideration in the design for the two-layer computer experiments is the trade-off between *exploration*

(\mathbf{X}_n must be space-filling to a certain degree) and *exploitation* (\mathbf{X}_n^{outer} should fill up the interesting domain of the outer computer model). Sequential design methods can solve this problem by iteratively selecting design points. Because the space-filling property of \mathbf{X}_n^{outer} depends on the complexity of the inner computer model, the proposed sequential strategy updates the design by “learning” the inner computer model and assessing the quality of \mathbf{X}_n^{outer} adaptively.

3 Sequential Mixed-distance Design

To assess the quality of \mathbf{X}_n^{outer} , a new mixed inter-site distance is introduced in Subsection 3.1. This distance takes into account both the inter-site distance between the inner computer outputs and the inter-site distance between the design variables. In Subsection 3.2, we introduce the maximum criterion and apply this criterion to query the points sequentially.

3.1 The Mixed-distance

Recall that $\mathbf{x}^{outer} = (\mathbf{x}, \mathbf{h}(\mathbf{x})) \in [0, 1]^K \times \mathbb{R}^L$ is an input of the outer computer model. Define $d_{i,j}^{outer}$ to be the inter-site distance between \mathbf{x}_i^{outer} and \mathbf{x}_j^{outer} :

$$d_{ij}^{outer} = d(\mathbf{x}_i^{outer}, \mathbf{x}_j^{outer}) = wd(\mathbf{h}_i, \mathbf{h}_j) + (1 - w)d(\mathbf{x}_i, \mathbf{x}_j), \quad (2)$$

where $w \in [0, 1]$ is a pre-specified weight; $d(\mathbf{h}_i, \mathbf{h}_j)$ measures the distance between $\mathbf{h}(\mathbf{x}_i)$ and $\mathbf{h}(\mathbf{x}_j)$, which is defined later; $d(\mathbf{x}_i, \mathbf{x}_j) = \left[\sum_{k=1}^K |x_{i,k} - x_{j,k}|^2 \right]^{1/2}$ is the Euclidean distance between \mathbf{x}_i and \mathbf{x}_j . Obviously, this distance is a weighted mixture of the inter-site distance of the inner computer inputs and outputs. We call this distance the *Mixed-distance*.

Next, we elaborate on the definition of $d(\mathbf{h}_i, \mathbf{h}_j)$. Since the inner computer model is expensive, only a limited number of inner computer experiments can be run. Hence,

inputs $\mathbf{h}(\mathbf{x})$ to the outer model are unknown if it is not evaluated at \mathbf{x} . To estimate $\mathbf{h}(\mathbf{x})$, a surrogate model can be built to mimic the inner computer model. In practice, the GP model is always used to build the surrogate model, which will lead to uncertainty about the unobserved $\mathbf{h}(\mathbf{x})$. Thus, the conventional (deterministic) distances are not suitable here because they ignore the uncertainty of the surrogate model. From Ortega-Jiménez et al. (2021), the L_2 metric $\left\{ \mathbb{E} \left[\sum_{l=1}^L |h_l(\mathbf{x}_i) - h_l(\mathbf{x}_j)|^2 \right] \right\}^{1/2}$ is a common choice to measure the distance between two random vectors. Since h_l and $h_{l'}, l \neq l' \in 1, \dots, L$ may be dependent, it requires the marginal distribution functions of $h_l, l = 1, \dots, L$ to evaluate this distance. Deriving these marginal distribution functions is a difficult task. To simplify the calculation of the distance, we perform a principal component analysis (PCA) by utilizing the singular value decomposition (SVD) of the scaled \mathbf{Y}_I^T . Then we replace $d(\mathbf{h}_i, \mathbf{h}_j)$ by the distance between the first L^{pc} independent principal component scores (PCs). Such measures have been used in several published studies, for example, Ding et al. (2002). In this work, we assume that L is not too large. Because in general, when L is relatively large, the finite inner computer outputs will not be overlapped or be very close to each other. Even though, another advantage of PCA is reducing the dimension of $\mathbf{h}(\cdot)$, thus further simplifying the calculation.

Let $\mathbf{Y}_I^{pc} = [\mathbf{H}_1^{pc}, \dots, \mathbf{H}_{L^{pc}}^{pc}]$ with $\mathbf{H}_l^{pc} = [h_l^{pc}(\mathbf{x}_1), \dots, h_l^{pc}(\mathbf{x}_n)]^T, l = 1, \dots, L^{pc}$ denote the L^{pc} uncorrelated PCs, and $L^{pc} < \min(L, n)$. Suppose h_l^{pc} is one realization of a GP. Measure the distance between $\mathbf{h}(\mathbf{x}_i)$ and $\mathbf{h}(\mathbf{x}_j)$ by using the following L_2 metric:

$$d(\mathbf{h}_i, \mathbf{h}_j) = \left\{ \mathbb{E} \left[\sum_{l=1}^{L^{pc}} |h_l^{pc}(\mathbf{x}_i) - h_l^{pc}(\mathbf{x}_j)|^2 \right] \right\}^{1/2}. \quad (3)$$

Since $d(\mathbf{x}_i, \mathbf{x}_j)$ and $d(\mathbf{h}_i, \mathbf{h}_j)$ are both valid L_2 metrics, the Mixed-distance (2) is a valid metric. In addition, for the PCs from the PCA procedures, the following conclusions hold (Jolliffe, 2002): (I) the Euclidean distance calculated using all L PCs is identical to that calculated from the scaled \mathbf{Y}_I^T ; (II) suppose that $L^{pc}(< L)$ PCs account for most of

the variation in the scaled \mathbf{Y}_I^T . Using L^{pc} PCs provide an approximation to the original Euclidean distance. As the original distance is calculated from the scaled \mathbf{Y}_I^T , the distance (3) used in this work set equal weights on each h_l^{pc} . That is, we don't scale the h_l^{pc} to $[0, 1]$ as Joseph and Hung (2008).

Next, we focus on the calculation of $d(\mathbf{h}_i, \mathbf{h}_j)$. By the assumptions on $h_l^{pc}, l = 1, \dots, L^{pc}$, independent GP models can be adapted to mimic the PCs. Details about the GP modeling can be found in Appendix A. Denote the posterior mean and variance functions of $h_l^{pc}(\mathbf{x}_i) - h_l^{pc}(\mathbf{x}_j)$, i.e., mean and variance functions of $h_l^{pc}(\mathbf{x}_i) - h_l^{pc}(\mathbf{x}_j)$ conditioned on $\mathbf{X}_n, \mathbf{Y}_I$, by $\mu_l(\mathbf{x}_i, \mathbf{x}_j)$ and $\tau_l^2(\mathbf{x}_i, \mathbf{x}_j)$, respectively. Based on the moments of normal distribution (Winkelbauer, 2012), it can be easily verified that the closed form solution of $d(\mathbf{h}_i, \mathbf{h}_j)$ is

$$d^2(\mathbf{h}_i, \mathbf{h}_j) = \sum_{l=1}^{L^{pc}} (\mu_l^2 + \tau_l^2). \quad (4)$$

Specifically, for any $\mathbf{x} \in [0, 1]^K$, there is $|\mu_l(\mathbf{x}, \mathbf{x}_i)| = |\hat{h}_l^{pc}(\mathbf{x}) - h_l^{pc}(\mathbf{x}_i)|$ and $\tau_l = s_l(\mathbf{x})$. Here, $\hat{h}_l^{pc}(\mathbf{x})$ is the GP predictor of h_l^{pc} at the point \mathbf{x} and $s_l(\mathbf{x})$ the standard deviation. The specific forms of $\hat{h}_l^{pc}(\mathbf{x})$ and $s_l(\mathbf{x})$ can be found in (16) and (17), respectively. Suppose $\hat{h}_l^{pc}(\mathbf{x}), l = 1, \dots, L^{pc}$ are a continuous function and differentiable on $[0, 1]^K$. This assumption can be guaranteed by chosen Gaussian correlation functions (13) and Matérn correlation functions (14) as the correlation functions. From one-order Taylor expansion of $h_l^{pc}(\mathbf{x})$ at $\mathbf{x}_i, i \in \{1, \dots, n\}$, we have that,

$$|\hat{h}_l^{pc}(\mathbf{x}) - h_l^{pc}(\mathbf{x}_i)| = \left| \frac{\partial \hat{h}_l^{pc}(\mathbf{x})}{\partial \mathbf{x}} \right| |\mathbf{x} - \mathbf{x}_i| + O(|\mathbf{x} - \mathbf{x}_i|^2).$$

Combining with the definition of the Mixed-distance (2), we have that larger distance between \mathbf{x} and $\mathbf{x}_i, i = 1, \dots, n$, larger absolute value of $\frac{\partial \hat{h}_l^{pc}(\mathbf{x})}{\partial \mathbf{x}}$ and larger $s_l(\mathbf{x})$ will deduce to larger Mixed-distance. A large absolute value of $\frac{\partial \hat{h}_l^{pc}(\mathbf{x})}{\partial \mathbf{x}}$ implies that the inner GP predictor varies drastically; a large $s_l(\mathbf{x})$ implies a large uncertainty of the GP predictor for the l -th PCs.

It is worth noticing that, a simpler alternative of the definition of $d(\mathbf{h}_i, \mathbf{h}_j)$ is a standard deterministic distance between just the posterior mean of the L^{pc} PCs. That is, for any unobserved $\mathbf{x} \in [0, 1]^K$, there is $d^2(\mathbf{h}_i, \mathbf{h}(\mathbf{x})) = \sum_{l=1}^{L^{pc}} [\hat{h}_l^{pc}(\mathbf{x}) - h_l^{pc}(\mathbf{x}_i)]^2$. Relative to this deterministic distance, the proposed one (4) considers the variance/uncertainty in the GP predictors for the PCs.

3.2 Maximin-distance design criterion

Johnson et al. (1990) showed that the maximin distance design is asymptotically optimum under a Bayesian setting. Moreover, this criterion optimizes the worst case, thus generating robust space-filling designs. We adopt the maximin distance criterion to query a sequential point, that is,

$$\mathbf{x}_{n+1} = \max_{\mathbf{x} \in [0, 1]^K} \min_{1 \leq i \leq n} w d(\mathbf{h}_i, \mathbf{h}(\mathbf{x})) + (1 - w) d(\mathbf{x}_i, \mathbf{x}). \quad (5)$$

The obtained sequential design is called *sequential mixed-distance design*, abbreviated as SMDD. The weight w balances the space-filling property of the two parts of outer computer inputs. If $w = 0$, \mathbf{x}_{n+1} is a sequential point that maximizes the minimal distance between \mathbf{x} and \mathbf{x}_i . If $w = 1$, the maximin distance property of \mathbf{h}_{n+1} is guaranteed, whereas the maximin distance property of \mathbf{x}_{n+1} is lost. The choice of w is a hard task because $d(\mathbf{h}_i, \mathbf{h}(\mathbf{x}))$ and $d(\mathbf{x}_i, \mathbf{x})$ have different scales.

A natural idea to avoid determining the weights is that we first pre-specify a set of candidate points, whose space-filling properties are guaranteed, and then obtain the sequential points by maximizing the minimum of $d(\mathbf{h}_i, \mathbf{h}(\mathbf{x}))$, that is,

$$\mathbf{x}_{n+1} = \max_{\mathbf{x} \in X_{cand}} \min_{1 \leq i \leq n} d(\mathbf{h}_i, \mathbf{h}(\mathbf{x})), \quad (6)$$

where X_{cand} is the set of candidate points. The choice of candidate points X_{cand} affects the accuracy and the efficiency of the optimization (6). Choosing points sequentially from a larger candidate set based on the maximin-design criterion (6) is commonly referred to as

the computer-aided design of experiment (CADEX) algorithm (Kennard and Stone, 1969). A very straightforward choice for X_{cand} is an LHD. To avoid sequentially adding points too close to existing points, we suggest using the sliced LHD (SLHD), such as sliced MmLHD (Ba et al., 2015), balanced sliced orthogonal arrays (Ai et al., 2014), the flexible sliced designs (Kong et al., 2018) and the sliced rotated sphere packing designs (He, 2019) etc. to generate the initial and the candidate points.

Because many different designs may have the same minimum inter-site distance, an extension of the maximin criterion is the ϕ_q criterion. This ϕ_q criterion minimizes the average reciprocal interpoint distance between the input points (Jin et al., 2005). Then (6) becomes

$$\mathbf{x}_{n+1} = \min_{\mathbf{x} \in X_{cand}} \phi_q, \quad (7)$$

where

$$\phi_q(\mathbf{x}) = \left\{ \sum_{1 \leq i \leq n} d(\mathbf{h}_i, \mathbf{h}(\mathbf{x}))^{-q} \right\}^{1/q}, \quad q > 0. \quad (8)$$

For large enough q , minimizing ϕ_q is equivalent to maximizing the minimum distance among the design points.

Let n_0 be the sample size of the initial design and N be the sample size of the final sequential design. An usually used stopping rule in the literature is the number of runs. Assume the sample size of the candidate points, which are used to choose the sequential design point is N_c . When the dimension of \mathbf{x} is large, it is reasonable to use more runs. This requires a large number of candidate points. Thus we suggest setting $N_c = a(N - n_0)K$, where a is a pre-specified constant. The corresponding procedure for generating the desired design can be described in Algorithm 1.

Note that, the PCs are obtained from the sample matrix \mathbf{Y}_I . As the iteration proceeds, the sample size of \mathbf{Y}_I increases, and the reasonable value for L^{pc} could generally become larger (Jolliffe, 2002). To ensure the stability of outcomes of principal components analysis,

Algorithm 1 Sequential LHD

Obtain an initial design \mathbf{X}_{n_0} with n_0 points, and run the inner computer simulator at these points, yielding the corresponding simulator outputs \mathbf{Y}_I ;

Generate N_c candidate samples, denoted as \mathcal{D}_c ;

for iteration $n = n_0, \dots, N - 1$ **do**

Centre the matrix \mathbf{Y}_I^T and denote as \mathbf{Y}_I^{*T} , so that the mean of each column of \mathbf{Y}_I^{*T} is zero, and the variance of each column is one;

Calculate the singular value decomposition of \mathbf{Y}_I^{*T} , i.e., $\mathbf{Y}_I^{*T} = S\mathbf{V}\mathbf{\Gamma}^T$, where $\mathbf{\Gamma}$ is an $L \times L$ unitary matrix containing the principal components (the eigenvectors), \mathbf{V} is an $n \times L$ diagonal matrix containing the ordered principal values (the eigenvalues), S is an $n \times n$ matrix containing the left singular values;

Choose L^{pc} such that the cumulative variation of the first L^{pc} PCs is more than 90% of total variation;

Project \mathbf{Y}_I^{*T} onto the principal subspace which is denoted as $[\mathbf{H}_1^{pc}, \dots, \mathbf{H}_{L^{pc}}^{pc}]$, where

$$\mathbf{H}_l^{pc} = [h_l^{pc}(\mathbf{x}_1), \dots, h_l^{pc}(\mathbf{x}_n)]^T, l = 1, \dots, L^{pc}$$

Build independent GP models to mimic $[\mathbf{H}_1^{pc}, \dots, \mathbf{H}_{L^{pc}}^{pc}]$;

Find $\mathbf{x}_{n+1} = \min_{\mathbf{x} \in \mathcal{D}_c} \phi_q(\mathbf{x})$;

Run the inner computer code at \mathbf{x}_{n+1} , augment \mathbf{X}_N and \mathbf{Y}_I with \mathbf{x}_{n+1} and $\mathbf{h}(\mathbf{x}_{n+1})$;

end for

return \mathbf{X}_N and \mathbf{Y}_I ;

the ratio n_0/L should be larger than 3 (Grossman et al., 1991). Considering the accuracy of GP models, we suggest the initial sample size $n_0 = \max(n_0^*, 3L)$, where n_0^* is the sample size that can guarantee the accuracy of the GP models. Besides, if the inner computer outputs can be mimicked by independent GP models, then the PCA can be omitted. n_0 is determined by n_0^* . The common choice of n_0^* is $10K$, as recommended in Loepky and Welch (2009).

4 Numerical Simulations

In this section, we compare the performance of three methods: (1) SMDD: the proposed sequential mixed-distance design; (2) SMDD-Det: sequential mixed-distance design when $d(\mathbf{h}_i, \mathbf{h}_j)$ is the standard deterministic distance between the $\hat{h}_l^{pc}(\mathbf{x})$ value; (3) MmLHD: maximin Latin hypercube design with the sample size equals to N . MmLHD does not depend on the initial design. The following two initial designs are considered for the SMDD and SMDD-Det.

- ID₁: The initial design \mathbf{X}_{n_0} is an MmLHD;
- ID₂: Poorly space-filled initial design, e.g., some parts of the design region are not explored.

Here, by comparing the performance of the first and the second method, we can explore the advantage of introducing the distance (3). Involving two initial designs can help us further understand the impact of the initial design and the accuracy of the inner GP models on the sequential designs.

The works of Marque-Pucheu et al. (2019) and Ming and Guillas (2021) assumed that both the inner and outer computer experiments are realizations of stationary GPs. A stationary GP assumes that the function of interest has the same degree of smoothness

in the whole covariate space. This assumption is too strong in many cases (Wang et al., 2022). Taking composite structure (aircraft) assembly as an example, the outer computer simulator describes the riveting process, which could be influenced by dynamic forces, varying input shape deviations, and generated residual stresses. For more details refer to the case study.

To obtain a design robust to the model assumption for the outer computer simulators, different from the optimal design (Marque-Pucheu et al., 2019; Ming and Guillas, 2021), the proposed method focuses on the space-filling property of the design for the outer computer experiments. The average inter-site distances (abbreviated as AID) of \mathbf{X}_N and \mathbf{Y}_I are used to compare the performance of different designs, which are defined as

$$AID_x = \frac{2}{N(N-1)} \sum_{i=1, i \leq j}^N \sum_{j=1}^N d(\mathbf{x}_i, \mathbf{x}_j),$$

$$AID_h = \frac{2}{N(N-1)} \sum_{i=1, i \leq j}^N \sum_{j=1}^N d(\mathbf{h}_i, \mathbf{h}_j),$$

It is obvious that the design with the larger AID is better for the same sample size.

For a fair comparison, we started the iteration with the initial sample size $n_0 = \max(10K, 3L)$. The stopping rule is set on the sample size of the final sequential design N . Set $N_c = 5(N - n_0)K$, the N_c candidate points are generated from the sliced MmLHD (Ba et al., 2015). The sequentially added point is then queried by minimizing $\phi_q(\mathbf{x})$ over the candidate points. Here q is set on 15 (Jin et al., 2005).

Example 1 *Suppose the inner computer simulator includes the three-hump Camel function and six-hump Camel function:*

$$h_1(\mathbf{x}) = 2\bar{x}_1^2 - 1.05\bar{x}_1^4 + \frac{\bar{x}_1^6}{6} + \bar{x}_1\bar{x}_2 + \bar{x}_2^2,$$

$$h_2(\mathbf{x}) = (4 - 2.1\bar{x}_1^2 + \frac{\bar{x}_1^4}{3})\bar{x}_1^2 + \bar{x}_1\bar{x}_2 + (-4 + 4\bar{x}_2^2)\bar{x}_2^2,$$

where $\bar{x}_1 = 2x_1 - 1$, $\bar{x}_2 = 2x_2 - 1$, $\mathbf{x} = (x_1, x_2) \in [0, 1]^2$.

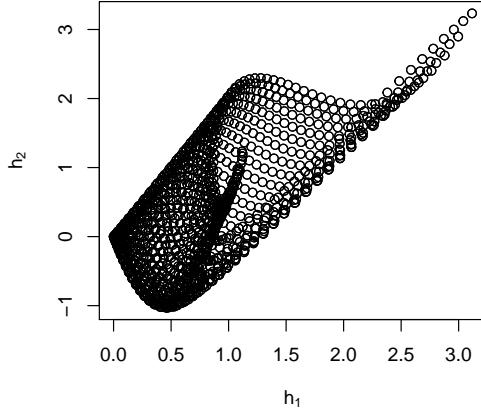


Figure 4: Outputs of the inner computer simulators.

Figure 4 illustrates the range of the inner computer outputs by conducting the inner computer experiments at 2000 MmLHD points. It can be seen that the inner computer outputs form a “knife-like” shape. It is hard to construct an LHD in such an irregular design region. Thus, the space-filling designs proposed by Kyzyurova et al. (2018), which build space-filling designs for the inner and outer computer experiments separately, are not sufficient. In addition, we can further see from Figure 4 that more of the inner computer outputs are located at the positions where h_1 and h_2 are small.

Set $n_0 = 20$ and $N = 2n_0$. By conducting PCA for the initial inner computer outputs, we have that the first PCs account for 84.80% of the total variation in the data, and two PCs account for 100% of the total variation. That is, $L^{pc} = L = 2$. By choosing Matérn correlation functions (14) with smoothness parameter $\nu = 5/2$ as correlation functions, two GP models are built to mimic the two PCs. Following Algorithm 1, Figure 5 shows the relationship between the uncertainty of the GP models and the locations of the sequential points by the proposed method under the initial design ID_1 . The first row is the contour plots of PC_1 and PC_2 . The second and the third row involve the contour plots of the

posterior mean and posterior variance of PC_1 and PC_2 , respectively. The red plus signs are sequentially added points generated by the proposed method. It can be seen that the

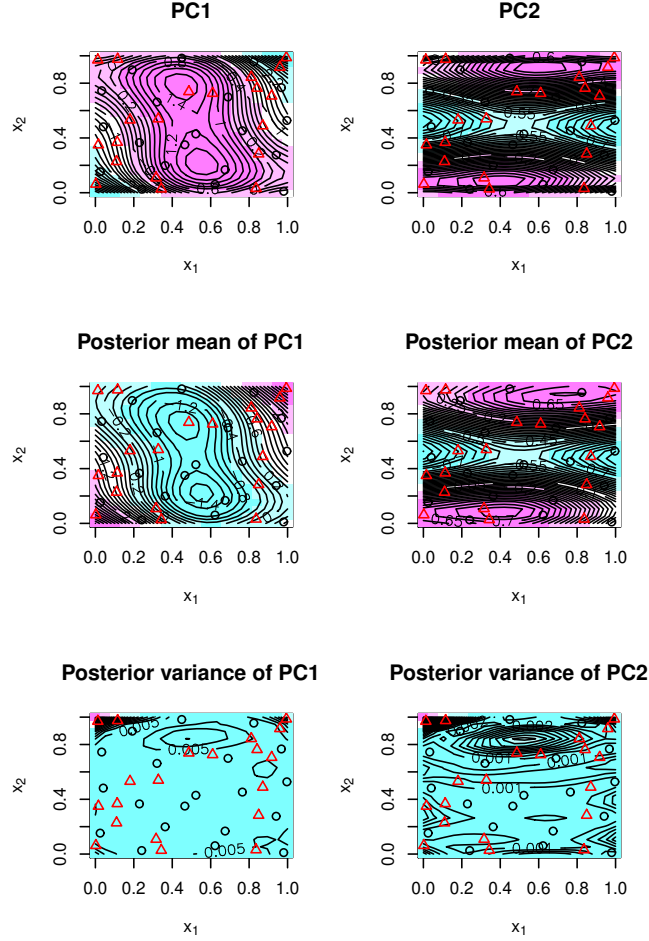


Figure 5: The first row: the contour plots of PC_1 and PC_2 . The second and the third row: the contour plots of the posterior mean and posterior variance of PC_1 and PC_2 , respectively. The red triangle signs are the sequentially added points by the proposed method.

sequentially added points are mainly concentrated in the places with the large absolute value of the derivatives and large posterior variance of the PCs.

The sequential designs obtained by three benchmark methods and the corresponding inner computer outputs are shown in Figure 6. By comparing the first column with others, we can see that the proposed method yields the most uniform design and the most uniform

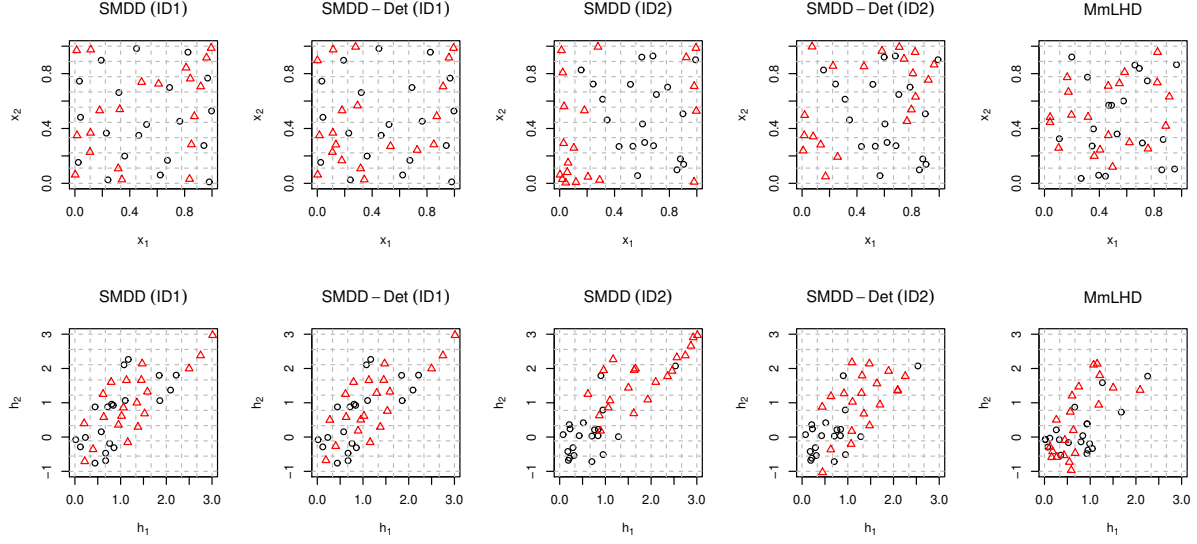


Figure 6: The sequential design points with $n_0 = 20$ and $N = 40$. The black circles are the initial points and the red triangles are the sequentially added points. The ID₁ in the first and the third columns refers to an initial MmLHD. The ID₂ in the second and the fourth columns indicate a poorly space-filled initial design, which doesn't explore the region $\{(x_1, x_2) \in [0, 1]^2 : x_1 + x_2 < 0.5\}$.

inner computer outputs. Specifically, because of ignoring the posterior variance of PC1 and PC2, the sequential points obtained by the second method (SMDD-Det) are mainly concentrated in the places with the large absolute value of the derivatives. Some locations with large posterior variance, such as the point located around $(0.6, 0.8)$ as shown in the first row and second column, are missed. Moreover, the design and the corresponding computer outputs in the first column (in the second column) are more space-filled than that in the third column (in the fourth column). It indicates that the sequential design under the initial design ID_1 outperforms the design under the initial design ID_2 . For the first method (SMDD), the poor initial design leads to large posterior variance at the unexplored region $\{(x_1, x_2) \in [0, 1]^2 : x_1 + x_2 < 0.5\}$. Thus more sequential points are added at this region, resulting in poor spaced-filled inner computer outputs. For the second method (SMDD-Det), the low accuracy of the GP models leads to the region $\{(h_1, h_2) : h_1 > 2.5, h_2 > 2.5\}$ unexplored. The results in the fifth column show that the design and the corresponding inner computer outputs obtained by the last method have the poorest uniformity because $N - n$ MmLHD points are added randomly to the initial n MmLHDs.

Denote the set of \tilde{N} test points as $\tilde{\mathbf{X}} = [\tilde{\mathbf{x}}_1, \dots, \tilde{\mathbf{x}}_{\tilde{N}}]^T$, which is a MmLHD. Let $\tilde{N} = 500$, after adding $j, j = 1, \dots, N - n_0$ sequential points, the following mean posterior variance (MPV) is used to evaluate the uncertainty of the GP models for the current PCs:

$$\text{MPV}_l = \frac{1}{\tilde{N}} \sum_{i=1}^{\tilde{N}} s_l^2(\tilde{\mathbf{x}}_i), l = 1, \dots, L^{pc}, \quad (9)$$

where $s_l^2(\tilde{\mathbf{x}})$ (17) is the posterior variance of the GP predictor for the current l -th PCs at testing point $\tilde{\mathbf{x}}$. Unlike the mean squared prediction error (MSPE), the MPV is only relevant to the location of $\tilde{\mathbf{x}}$. It is not necessary to run the computer experiment at $\tilde{\mathbf{x}}$, so this criterion is also applicable to expensive computer experiments. Figure 7 shows the variation of mean posterior variance for the two PCs as the number of sequential points increases.

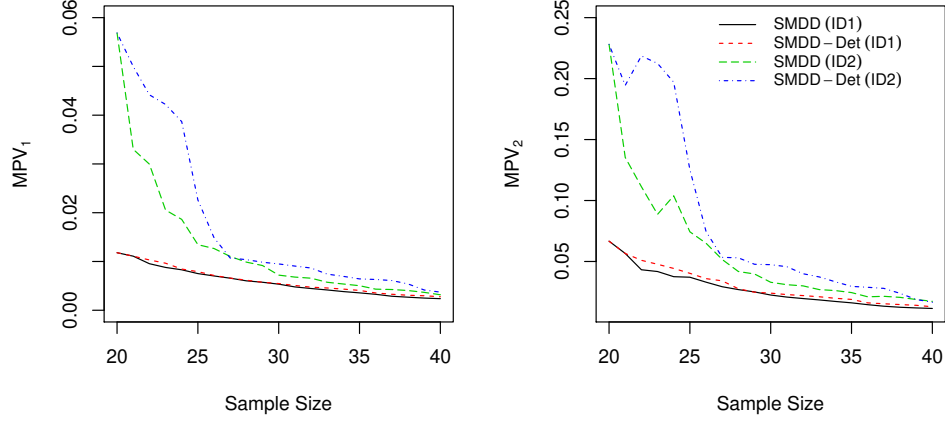


Figure 7: MPV of the GP models for the two PCs v.s. the sample size as the number of sequential points increases.

It can be seen that the GP predictors for the two PCs under the initial design ID₁ are much more accurate than the predictors under the initial design ID₂. Since the proposed method considers the uncertainties of the GP predictors, the accuracy of the GP models under the proposed design is increased more quickly than that under the design given by the second method.

To further examine whether the proposed design can help to improve the prediction accuracy of the outer surrogate model, we use the mean posterior variance (MPV) of the outer predictor to compare the accuracy of the outer surrogate model under different designs. Two kinds of outer surrogate models, including a stationary GP model and a non-GP or a non-stationary GP model (here we use the Neural Network model), are used to illustrate that the proposed design is robust to the model assumption for the outer computer simulators.

- GP model. Suppose the outer computer model is the modified Branin-Hoo function

$$g(h_1, h_2) = \left(h_2 - \frac{5.1}{4\pi^2} h_1^2 + \frac{5}{\pi} h_1 - 6 \right)^2 + 10 \left(1 - \frac{1}{8\pi} \right) \cos(5h_1) + 10,$$

$$(h_1, h_2) \in [-5, 10] \times [0, 15].$$

By choosing the Matérn correlation functions (14) with smoothness parameter $\nu = 5/2$ as correlation functions, a GP model is used to mimic the Branin-Hoo function.

- Neural Network model. Suppose the outer computer model is a two-dimensional zigzag function

$$g(h_1, h_2) = h_1 + 2h_2 - \lfloor 0.5 + h_1 \rfloor - \lfloor 0.4 + h_2 \rfloor, h_1, h_2 \in [0, 1]^2.$$

The zigzag is difficult to approximate by a stationary GP model because of its non-differentiable points (Lee et al., 2020). With the help of the R package *neuralnet* (Fritsch et al., 2016), a Neural Network model of depth 3 is built to approximate the zigzag function.

The test points are sampled from the 2000 MmLHD points as shown in Figure 4, so that the inner computer outputs at the testing points are space-filled in the “knife-like” region. Comparison of the accuracy of the GP predictors and the Neural Network predictors are shown in Figure 8. It can be seen that under the designs given by the proposed method, the GP and the Neural Network predictors for the outer computer simulators perform best. It indicates that the proposed method is robust to the model assumption for the outer computer simulators. The third method yields the worst-performing design. Moreover, the design given by the third method will lead to a singular covariance matrix of the GP model as more sequential points are added. It shows that the third method is not suitable for the design of nested computer experiments if the outer simulator is mimicked by a GP model.

By repeating Algorithm 1 for 100 times, Figure 9 shows the mean of the AID of \mathbf{X}_N and \mathbf{Y}_I with different sample size N of the final sequential design. It can be seen that the proposed design outperforms all other methods when the sample size becomes large. From Figure 6, we have that, the sequential points are located at the boundary of the

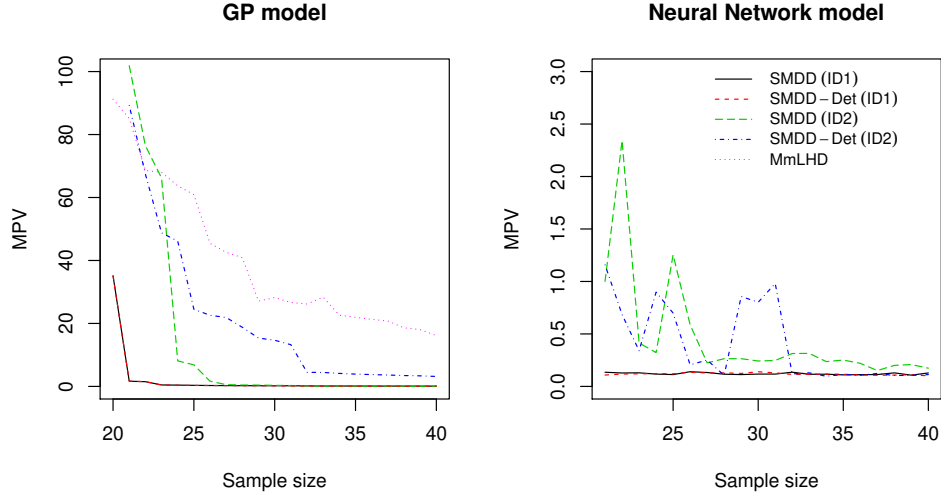


Figure 8: MPV of the GP predictors (left) and MPV of the Neural Network predictors (right) v.s. the sample size as the number of sequential points increases. (MPV of the Neural Network predictor under the last design is not shown because it is too large.)

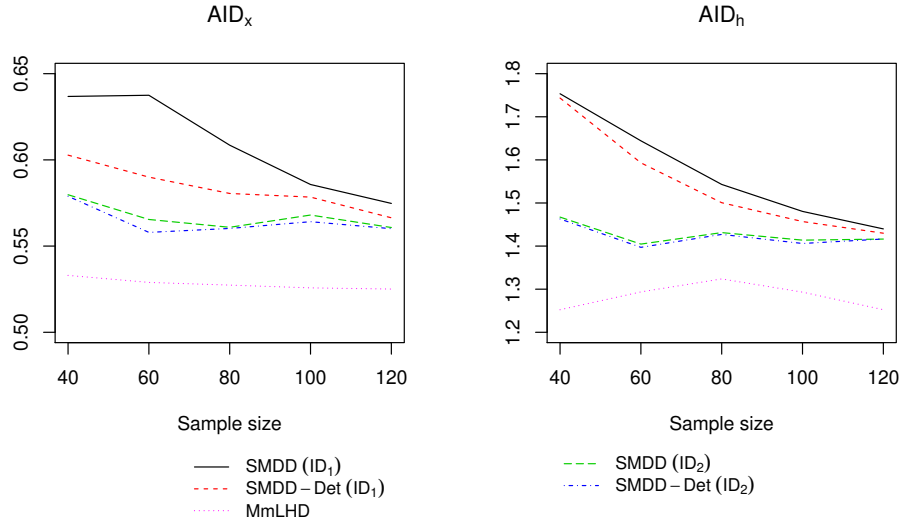


Figure 9: The AID of \mathbf{X}_N (left) and \mathbf{Y}_I (right) v.s. the final sample size N , with fixed $n_0 = 20$ and $N_c = 5(N - n_0)K = 10(N - n_0)$.

experimental space, such as the lower-left corner and the upper-right corner. It makes the AID_x for the sequential designs generated by the first two methods increase first and then decrease. With the further increase of the sample size, the AID_h will gradually decrease. By comparing the performance of the first two methods under the same initial design, we have that, under the initial design ID_1 , the proposed method achieves the largest average inter-site distance as the sample size becomes large. The third method yields the worst-performing design.

Example 2 (A high-dimensional example) *Suppose the outputs of the inner computer simulator at the point \mathbf{x} are 10 dimensional, and the l -th output is*

$$h_l(\mathbf{x}) = 4a_{l1}(x_1 - 2 + 8x_2 - 8x_2^2)^2 + a_{l2}(3 - 4x_2)^2 + 16a_{l3}\sqrt{x_3 + 1}(2x_3 - 1)^2 + a_{l4} \sum_{i=1}^8 i \ln(1 + \sum_{j=3}^i x_j), \mathbf{x} \in [0, 1]^8, \quad (10)$$

where the parameters $a_{lj}, l = 1, \dots, 10; j = 1, \dots, 4$ is pre-fixed on $A = \{a_{lj}\}$ with

$$A^T = \begin{bmatrix} 0.614 & 0.453 & 0.264 & 0.354 & 0.850 & 0.514 & 0.040 & 0.958 & 0.142 & 0.717 \\ 0.965 & 0.400 & 0.189 & 0.574 & 0.323 & 0.791 & 0.093 & 0.813 & 0.617 & 0.221 \\ 0.761 & 0.410 & 0.691 & 0.872 & 0.248 & 0.574 & 0.386 & 0.086 & 0.135 & 0.938 \\ 0.296 & 0.189 & 0.561 & 0.775 & 0.945 & 0.002 & 0.356 & 0.615 & 0.819 & 0.435 \end{bmatrix}. \quad (11)$$

Let $n_0 = \max(10K, 3L) = 80$. The inner computer experiments are conducted at n_0 MmLHDs. The pairwise correlation between the 10 vectors of inner computer outputs are shown in Figure 10. From the pairwise correlation plot (Figure 10), we have that most of the inner computer outputs are highly correlated with the others. By performing SVD decomposition on the initial scaled \mathbf{Y}_I , we have that the first two PCs account for more than 90% of the total variation in the data.

By choosing Matérn correlation functions (14) with smoothness parameter $\nu = 5/2$ as correlation functions, two GP models are built to mimic the PCs. Figure 11 shows the

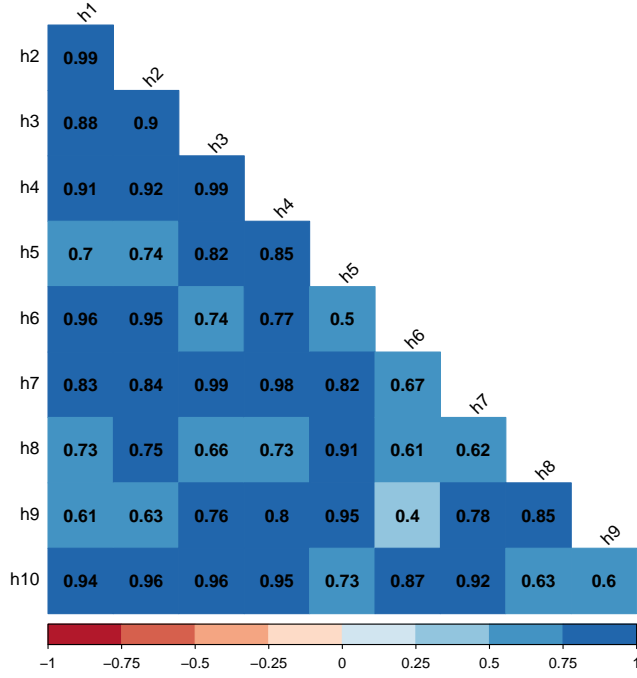


Figure 10: The pairwise correlation of $\{h_l\}_{l=1,\dots,10}$.

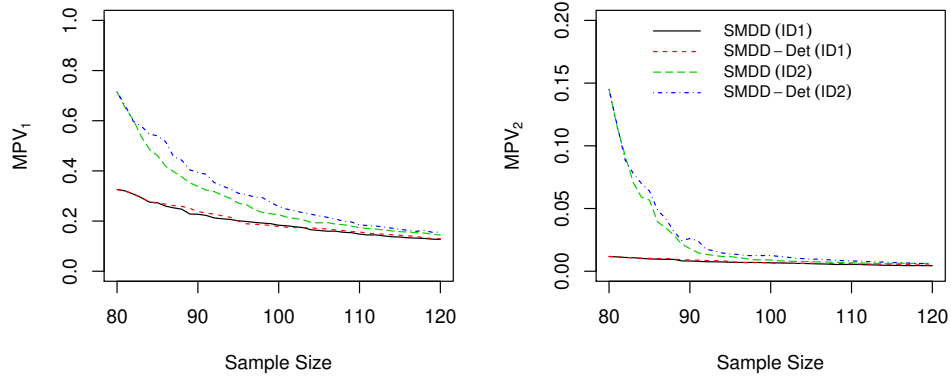


Figure 11: MPV of the GP models for the two PCs v.s. the sample size, as the number of sequential points increases.

variation of the MPV of the first two PCs as the number of sequential points increases. It can be seen that the GP models for the two PCs under the initial design ID_1 are much more accurate than the models under the initial design ID_2 . As 40 sequential points are added, the accuracy of the GP models under the design given by different methods tends to be the same.

Since the dimension of the inner computer output is 10, building a non-stationary GP model or a non-Gaussian process model for the outer simulator is very time-consuming. We only show the comparison results in the cases where the outer simulator can be approximated by a stationary GP model in this example. Suppose the outer computer model is the wing weight function (Sobester et al., 2008). By choosing the Matérn correlation functions (14) with smoothness parameter $\nu = 5/2$ as correlation functions, a GP model is used to mimic this function. A comparison of the accuracy of the GP predictors is shown in Figure 12. It can be seen that, under the designs given by the proposed method, the

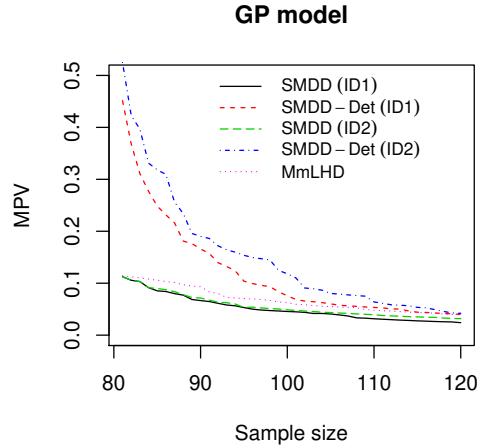


Figure 12: MPV of the GP predictors v.s. the sample size as the number of sequential points increases.

outer GP predictor performs best.

By repeating Algorithm 1 for 100 times, Figure 13 shows the mean of the AID of \mathbf{X}_N and \mathbf{Y}_I with different sample size N of the final sequential design. Due to the large dimension

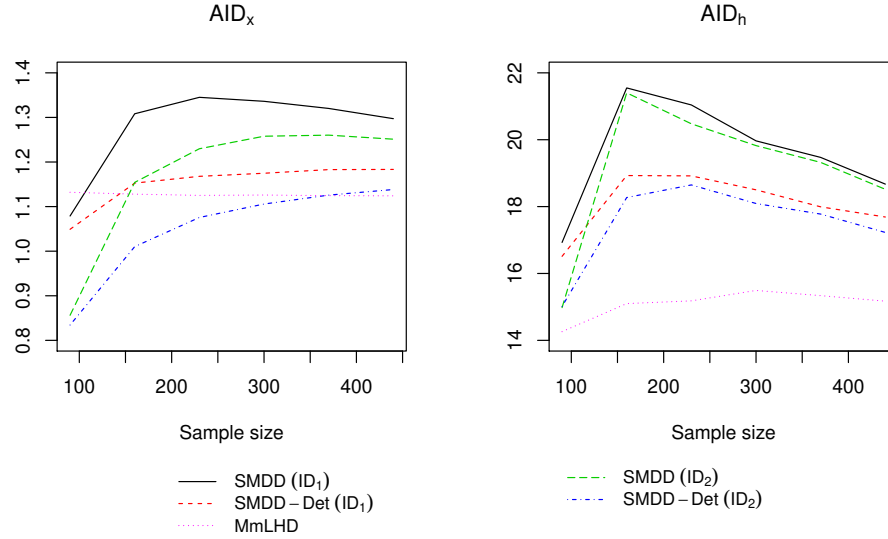


Figure 13: AID of \mathbf{X}_N and \mathbf{Y}_I v.s. the final sample size N .

of \mathbf{x} , when the sample size increases by 250, $\text{AID}_{x,s}$ of the first two methods still don't have a very obvious decrease trend. For the third method, $\text{AID}_{x,s}$ continue to decrease with the increase of sample size, although the decrease is not significant. The AID_h of the design given by the proposed method is larger than those of other methods, which illustrates the advantages of the proposed method. By comparing the first two methods under different initial designs, it can be seen that the poor initial design yields smaller AIDs. As the sample size increases, the difference from the initial design diminishes. By comparing the performance of the first two methods under the same initial design, we have that, under the initial design ID_1 , the proposed method achieves the largest average inter-site distance as the sample size becomes large. The third method yields the smallest average inter-site distance for both \mathbf{X}_N and \mathbf{Y}_I . Combined with Figure 12, we have that designs with large AID lead to more accurate predictions.

5 Composite Structure Assembly Experiments

In this section, we apply the proposed design to the computer simulation for the composite structures assembly process. As mentioned in Section 1, the composite structure assembly simulation involves two-layer computer models. The inner computer model is the Automatic Optimal Shape Control (AOSC) system that adjusts one fuselage (named part 1) to the target shape (assumed to be the shape of the other fuselage, named part 2) by ten actuators. After the shape adjustment, the two fuselages are assembled by the riveting process. Then, the actuators applied on the two fuselages will be released. It will cause the spring-back of the fuselages and the occurrence of residual stress. Residual stress may hurt the parts as well as generate other severe side effects (e.g., fatigue, stress corrosion cracking, and structural instability)(Wen et al., 2019). Therefore, the outer computer model is the platform that evaluates the residual stress during and after the assembly process. Table 1 summarizes the inputs and outputs information in this computer experiment.

Table 1: Inputs and outputs for the two-layer computer experiments		
Inner computer model		
	Name of variable	Dimension
Inputs	Part 1's actuators' forces (\mathbf{x})	$K = 10$
Outputs	Part 1's critical dimensions ($\mathbf{h}(\mathbf{x})$)	$L = 53$
Outer computer model		
	Name of variable	Dimension
Inputs	Part 1's critical dimensions ($\mathbf{h}(\mathbf{x})$)	$L = 53$
Outputs	Maximum of the Stress	$M = 1$

Since the composite structure assembly experiments are very time-consuming, it is assumed that the maximum sample size for the computer experiments is 100 (Yue et al., 2018). Obviously, $3L$ is larger than 100. It means that the sample size for the initial design cannot be set at $\max(10K, 3L)$. From Yue et al. (2018), building GP models for each $h_l, l = 1, \dots, 53$ independently with $n_0^* = 30$ training data can achieve satisfactory

prediction performance. As a result, we ignore the correlation between the outputs. The PCA for the inner computer outputs \mathbf{Y}_I can be omitted and only the accuracy of the GP models needs to be considered when choosing n_0 . Set $n_0 = n_0^* = 30$, and $N = 100$. Figure 14 shows the mean of 53 MPVs as the number of sequential points increases. It can be seen

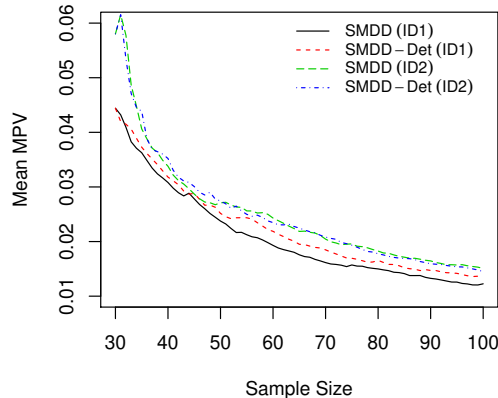


Figure 14: Mean of the L MPVs for the independent GP models as the number of sequential points increases.

that the uncertainty of the 53 GP models under the proposed design is smaller. As the sample size increases, the differences introduced by the different initial designs decrease.

Due to the impact of arithmetic power, we only show the average inter-site distance obtained by running Algorithm 1 once. Figure 15 shows the mean of the AIDs of \mathbf{X}_N and \mathbf{Y}_I with different sample size N of the final sequential design. Due to the high dimensionality of \mathbf{x} and \mathbf{h} , AIDs for the first two methods don't have a significant decreasing trend with $N = 100$. The proposed design outperforms all other methods when the sample size becomes large. By comparing the first two methods under different initial designs, it can be seen that when the sample size is small, AID_h s under the second initial design are much smaller, due to the larger uncertainty of the GP models. By comparing the performance of

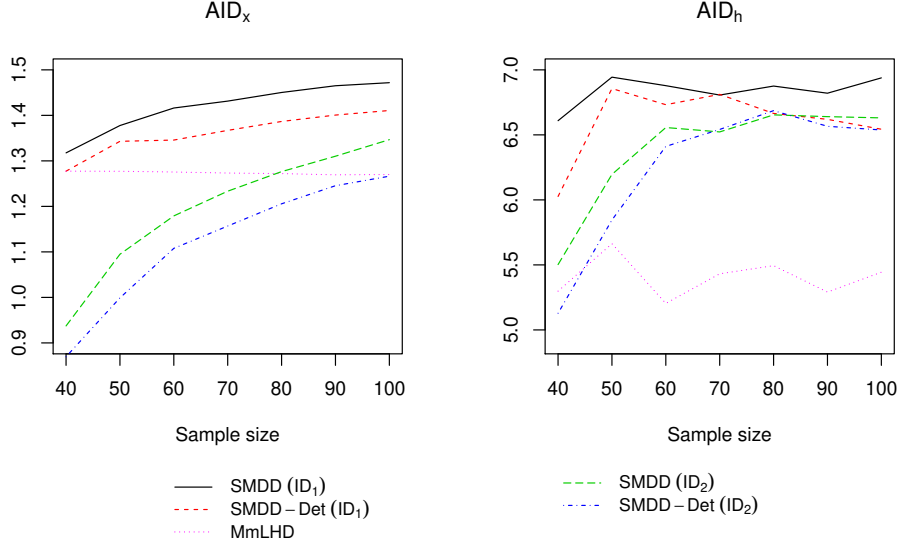


Figure 15: AID of \mathbf{X}_N and \mathbf{Y}_I v.s. the final sample size N .

the first two methods under the same initial design, we have that, under the initial design ID_1 , the proposed method achieves the largest average inter-site distance as the sample size becomes large. The third method yields the worst-performing design.

6 Conclusion and Discussion

In this work, we proposed a sequential design procedure for the two-layer computer experiments. The proposed design considers the space-filling property of both the inputs and the outputs for the inner computer experiments. A new sequential algorithm for efficiently generating such designs is also given. The numerical simulation results show the proposed design out-performance of the benchmark designs. At last, the proposed method is applied to generate designs for the composite structures assembly experiments.

The proposed method is robust to the assumption for the outer computer simulators but relies on the accuracy of the surrogate model for the inner computer simulator. An inner computer model-independent design approach will be considered later.

Supplementary Material

The data in case study and the corresponding R codes are available which are provided in the Supplementary Material. All files consist the .zip file.

Appendix A Gaussian Process models

In this section, we briefly introduce the GP modeling for the l -th PCs, $l = 1, \dots, L^{pc}$.

Suppose $h_l^{pc}(\cdot)$ is one realization of the GP

$$\begin{aligned} h_l^{pc}(\cdot) &= \boldsymbol{\beta}^T \mathbf{b}(\cdot) + Z(\cdot), \\ Z(\cdot) | \theta &\sim GP(0, \sigma^2 R(\cdot, \cdot)). \end{aligned} \quad (12)$$

$\mathbf{b}(\cdot)$ consists of q basis functions; $\boldsymbol{\beta}$ is the corresponding regression coefficients; $GP(0, \sigma^2 R)$ denotes a stationary GP with mean zero, covariance function $\sigma^2 R(\cdot, \cdot)$. Here, $\sigma^2 > 0$ is the variance and $R(\cdot, \cdot)$ is the correlation function. Common choices of $R(\cdot, \cdot)$ include the Gaussian correlation functions with

$$R(\mathbf{x}, \mathbf{x}') = \exp(-\theta \|\mathbf{x} - \mathbf{x}'\|), \quad (13)$$

and the Matérn correlation functions with

$$R(\mathbf{x}, \mathbf{x}') = \frac{1}{\Gamma(\nu)} \left(\frac{2\sqrt{\nu} \|\mathbf{x}_i - \mathbf{x}_j\|}{\theta} \right)^\nu K_\nu \left(\frac{2\sqrt{\nu} \|\mathbf{x} - \mathbf{x}'\|}{\theta} \right), \quad (14)$$

where $\theta > 0$ is the correlation parameter and K_ν denotes the modified Bessel function of the second kind with order ν .

Recall the inner computer experiments are conducted at the points $\mathbf{X}_n = (\mathbf{x}_1, \dots, \mathbf{x}_n)^T$ and the corresponding outputs of h_l^{pc} are $\mathbf{H}_l^{pc} = [h_l^{pc}(\mathbf{x}_1), \dots, h_l^{pc}(\mathbf{x}_n)]^T$. Denote $\mathbf{R} = R(\mathbf{X}_n, \mathbf{X}_n)$; $\mathbf{r}(\mathbf{x}) = R(\mathbf{x}, \mathbf{X}_n)$ and $\mathbf{B}^T = [\mathbf{b}(\mathbf{x}_1), \dots, \mathbf{b}(\mathbf{x}_n)]$. Given data $(\mathbf{X}_n, \mathbf{H}_l^{pc})$, the posterior distribution of $h_l^{pc}(\mathbf{x})$ is

$$h_l^{pc}(\mathbf{x}) | \mathbf{X}_n, \mathbf{H}_l^{pc} \sim N \left(\hat{h}_l^{pc}(\mathbf{x}), s_l^2(\mathbf{x}) \right). \quad (15)$$

Here, the posterior mean is

$$\hat{h}_l^{pc}(\mathbf{x}) = \hat{\boldsymbol{\beta}}^T \mathbf{b}(\mathbf{x}) + (\mathbf{Y}_I - \mathbf{B}\hat{\boldsymbol{\beta}})^T \mathbf{R}^{-1} \mathbf{r}(\mathbf{x}), \quad (16)$$

and the posterior variance is

$$s_l^2(\mathbf{x}) = \hat{\sigma}^2 \tilde{R}(\mathbf{x}, \mathbf{x}), \quad (17)$$

with

$$\tilde{R}(\mathbf{x}, \mathbf{x}') = R(\mathbf{x}, \mathbf{x}') - \mathbf{r}^T(\mathbf{x}) \mathbf{R}^{-1} \mathbf{r}(\mathbf{x}') + \mathbf{U}^T(\mathbf{x}) (\mathbf{B}^T \mathbf{R}^{-1} \mathbf{B})^{-1} \mathbf{U}(\mathbf{x}'),$$

and

$$\hat{\sigma}^2 = (n - 1)^{-1} (\mathbf{H}_l^{pc} - \mathbf{B}\hat{\boldsymbol{\beta}})^T \mathbf{R}^{-1} (\mathbf{H}_l^{pc} - \mathbf{B}\hat{\boldsymbol{\beta}}).$$

Here, $\hat{\boldsymbol{\beta}} = (\mathbf{B}^T \mathbf{R}^{-1} \mathbf{B})^{-1} \mathbf{B}^T \mathbf{R}^{-1} \mathbf{H}_l^{pc}$ and $\mathbf{U}(\mathbf{x}) = \mathbf{b}(\mathbf{x}) - \mathbf{B}^T \mathbf{R}^{-1} \mathbf{r}(\mathbf{x})$. In addition, the hyper-parameter θ in the correlation function is always unknown in practice, maximum likelihood estimators (MLEs) can be plugged into (15) to obtain the posterior distribution of h_k .

References

- Ai, M., B. Jiang, and K. Li (2014). Construction of sliced space-filling designs based on balanced sliced orthogonal arrays. *Statistica Sinica* 24(4), 1685–1702.
- Ba, S., W. R. Myers, and W. A. Brenneman (2015). Optimal sliced latin hypercube designs. *Technometrics* 57(4), 479–487.
- Chen, J., S. Mak, V. R. Joseph, and C. Zhang (2021). Function-on-function kriging, with applications to three-dimensional printing of aortic tissues. *Technometrics* 63(3), 384–395.

- Ding, C., X. He, H. Zha, and H. D. Simon (2002). Adaptive dimension reduction for clustering high dimensional data. In *2002 IEEE International Conference on Data Mining, 2002. Proceedings.*, pp. 147–154. IEEE.
- Fritsch, S., F. Guenther, and M. F. Guenther (2016). Package ‘neuralnet’. *The Comprehensive R Archive Network*.
- Grossman, G. D., D. M. Nickerson, and M. C. Freeman (1991). Principal component analyses of assemblage structure data: utility of tests based on eigenvalues. *Ecology* 72(1), 341–347.
- He, X. (2019). Sliced rotated sphere packing designs. *Technometrics* 61(1), 66–76.
- Jin, R., W. Chen, and A. Sudjianto (2005). An efficient algorithm for constructing optimal design of computer experiments. *Journal of Statistical Planning and Inference*, 134, 268–287.
- Johnson, M. E., L. M. Moore, and D. Ylvisaker (1990). Minimax and maximin distance designs. *Journal of statistical planning and inference* 26(2), 131–148.
- Jolliffe, I. T. (2002). *Principal component analysis for special types of data*. Springer.
- Joseph, V. R. and Y. Hung (2008). Orthogonal-maximin latin hypercube designs. *Statistica Sinica* 18(1), 171–186.
- Kennard, R. W. and L. A. Stone (1969). Computer aided design of experiments. *Technometrics* 11(1), 137–148.
- Kong, X., M. Ai, and K. L. Tsui (2018). Flexible sliced designs for computer experiments. *Annals of the Institute of Statistical Mathematics* 70(3), 631–646.

- Kyzyurova, K. N., J. O. Berger, and R. L. Wolpert (2018). Coupling computer models through linking their statistical emulators. *SIAM/ASA Journal on Uncertainty Quantification* 6(3), 1151–1171.
- Lee, C., J. Wu, W. Wang, and X. Yue (2020). Neural network gaussian process considering input uncertainty for composite structure assembly. *IEEE/ASME Transactions on Mechatronics* 27(3), 1267–1277.
- Loeppky, J. L. and S. W. J. Welch (2009). Special issue on computer modeling — choosing the sample size of a computer experiment: A practical guide. *Technometrics* 51(4), 366–376.
- Marque-Pucheu, S., G. Perrin, and J. Garnier (2019). Efficient sequential experimental design for surrogate modeling of nested codes. *ESAIM: Probability and Statistics* 23, 245–270.
- Ming, D. and S. Guillas (2021). Linked gaussian process emulation for systems of computer models using matérn kernels and adaptive design. *SIAM/ASA Journal on Uncertainty Quantification* 9(4), 1615–1642.
- Nicholls, S. D. and S. G. Decker (2015). Impact of coupling an ocean model to wrf nor’easter simulations. *Monthly Weather Review* 143(12), 4997–5016.
- Ortega-Jiménez, P., M. A. Sordo, and A. Suárez-Llorens (2021). Stochastic comparisons of some distances between random variables. *Mathematics* 9(9), 981.
- Santner, T. J., B. J. Williams, and W. I. Notz (2018). *The Design and Analysis Computer Experiments*. Springer New York.
- Shi, J. (2006). *Stream of variation modeling and analysis for multistage manufacturing processes*. CRC press.

- Sobester, A., A. Forrester, and A. Keane (2008). *Engineering design via surrogate modelling: a practical guide*. John Wiley & Sons.
- Ulrich, T., S. Vater, E. H. Madden, J. Behrens, Y. van Dinther, I. Van Zelst, E. J. Fielding, C. Liang, and A.-A. Gabriel (2019). Coupled, physics-based modeling reveals earthquake displacements are critical to the 2018 palu, sulawesi tsunami. *Pure and Applied Geophysics* 176(10), 4069–4109.
- Wang, Y., M. Wang, A. AlBahar, and X. Yue (2022). Nested bayesian optimization for computer experiments. *IEEE/ASME Transactions on Mechatronics*.
- Wang, Y., X. Yue, R. Tuo, J. H. Hunt, J. Shi, et al. (2020). Effective model calibration via sensible variable identification and adjustment with application to composite fuselage simulation. *Annals of Applied Statistics* 14(4), 1759–1776.
- Wen, Y., X. Yue, J. H. Hunt, and J. Shi (2018). Feasibility analysis of composite fuselage shape control via finite element analysis. *Journal of Manufacturing Systems* 46, 272–281.
- Wen, Y., X. Yue, J. H. Hunt, and J. Shi (2019). Virtual assembly and residual stress analysis for the composite fuselage assembly process. *Journal of Manufacturing Systems* 52, 55–62.
- Winkelbauer, A. (2012). Moments and absolute moments of the normal distribution. *arXiv preprint arXiv:1209.4340*.
- Yue, X., Y. Wen, J. H. Hunt, and J. Shi (2018). Surrogate model-based control considering uncertainties for composite fuselage assembly. *Journal of Manufacturing Science and Engineering* 140(4), 041017.